Atmos. Chem. Phys., 19, 1195–1206, 2019
https://doi.org/10.5194/acp-19-1195-2019

Atmospheric Chemistry and Physics
Open Access
EGU

In-cloud formation of secondary species in iron-containing particles

Qinhao Lin[1], Xinhui Bi[1], Guohua Zhang[1], Yuxiang Yang[1,2], Long Peng[1,2], Xiufeng Lian[1,2], Yuzhen Fu[1,2], Mei Li[3], Duohong Chen[4], Mark Miller[5], Ji Ou[6], Mingjin Tang[1], Xinming Wang[1], Ping'an Peng[1], Guoying Sheng[1], and Zhen Zhou[3]

[1]State Key Laboratory of Organic Geochemistry and Guangdong Key Laboratory of Environmental Resources Utilization and Protection, Guangzhou Institute of Geochemistry, Chinese Academy of Sciences, Guangzhou 510640, P. R. China
[2]University of Chinese Academy of Sciences, Beijing 100039, P. R. China
[3]Institute of Mass Spectrometer and Atmospheric Environment, Jinan University, Guangzhou 510632, P. R. China
[4]State Environmental Protection Key Laboratory of Regional Air Quality Monitoring, Guangdong Environmental Monitoring Center, Guangzhou 510308, P. R. China
[5]Department of Environmental Sciences, Rutgers, the State University of New Jersey, New Brunswick, NJ 08901, USA
[6]Shaoguan Environmental Monitoring Center, Shaoguan 512026, P. R. China

Correspondence: Xinhui Bi (bixh@gig.ac.cn)

Received: 29 August 2018 – Discussion started: 8 October 2018
Revised: 10 January 2019 – Accepted: 21 January 2019 – Published: 30 January 2019

Abstract. The increase in secondary species through cloud processing potentially increases aerosol iron (Fe) bioavailability. In this study, a ground-based counterflow virtual impactor coupled with a real-time single-particle aerosol mass spectrometer was used to characterize the formation of secondary species in Fe-containing cloud residues (dried cloud droplets) at a mountain site in southern China for nearly 1 month during the autumn of 2016. Fe-rich, Fe-dust, Fe-elemental carbon (Fe-EC), and Fe-vanadium (Fe-V) cloud residual types were obtained in this study. The Fe-rich particles, related to combustion sources, contributed 84 % (by number) to the Fe-containing cloud residues, and the Fe-dust particles represented 12 %. The remaining 4 % consisted of the Fe-EC and Fe-V particles. It was found that above 90 % (by number) of Fe-containing particles had already contained sulfate before cloud events, leading to no distinct change in number fraction (NF) of sulfate during cloud events. Cloud processing contributed to the enhanced NFs of nitrate, chloride, and oxalate in the Fe-containing cloud residues. However, the in-cloud formation of nitrate and chloride in the Fe-rich type was less obvious relative to the Fe-dust type. The increased NF of oxalate in the Fe-rich cloud residues was produced via aqueous oxidation of oxalate precursors (e.g., glyoxylate). Moreover, Fe-driven Fenton reactions likely increase the formation rate of aqueous-phase OH, improving the conversion of the precursors to oxalate in the Fe-rich cloud residues. During daytime, the decreased NF of oxalate in the Fe-rich cloud residues was supposed to be due to the photolysis of Fe-oxalate complexes. This work emphasizes the role of combustion Fe sources in participating in cloud processing and has important implications for evaluating Fe bioavailability from combustion sources during cloud processing.

1 Introduction

Iron (Fe)-containing particles were frequently detected in the atmosphere, with concentration ranging from 10 ng m^{-3} over remote marine environments to 28 µg m^{-3} near desert areas (Zhang et al., 2003; Fomba et al., 2013). The Fe-containing particles have an adverse effect on human health, causing issues such as DNA strand breakage and cell damage (See et al., 2007; Abbaspour et al., 2014). Some researchers also reported that Fe solubility might be an important criterion for toxicity in lung fluid (Costa and Dreher, 1997). Bioavailable Fe derived from atmospheric aerosol deposition can limit the photosynthetic activity of marine phytoplankton in high-nutrient low-chlorophyll waters, indirectly affects oceanic carbon uptake and storage, and has feedback effects on climate (Jickells et al., 2005). The Fe-containing particles can contain various species, such as calcium (Ca), silicon (Si),

aluminum (Al), vanadium (V), elemental carbon (EC), and secondary inorganic and organic species (Zhang et al., 2014; Bi et al., 2016; Dall'Osto et al., 2016). The presence and coexistence of various species could further modify the effects of the Fe-containing particles on human health, ecology, and climate (Mahowald et al., 2005; Abbaspour et al., 2014).

The Fe-containing particle sources mainly include mineral dust and combustion emissions (e.g., biomass burning, coal combustion, and iron/steel industrial activities) (Jickells et al., 2005; Sedwick et al., 2007). Abundant Ca, Si, and Al often exist in the Fe-containing particles from mineral dust sources (Sullivan et al., 2007a), while the Fe-containing particles from combustion sources usually contain EC and other metals, as well as minor amounts of Ca (Li et al., 2013; Dall'Osto et al., 2016). The chemical properties of the Fe-containing particles depend on its emission sources and could also be modified by the formation of secondary species during atmospheric processes (Zhang et al., 2014; Dall'Osto et al., 2016; Lin et al., 2017). The Fe-containing particles in East Asian outflows were often observed to be internally mixed with sulfate, mostly due to the large amount of SO_2 from coal in China (Furutani et al., 2011; Moffet et al., 2012; Li et al., 2013). Sullivan et al. (2007a) proposed that the enrichment of sulfate in the Asian mineral dust was possibly due to the Fe-catalyzed oxidation of SO_2 to sulfate. In European urban areas, Dall'Osto et al. (2016) found that the Fe-containing particles were internally mixed with nitrate rather than sulfate and were most likely associated with urban traffic activities. The frequent measurement of oxalate in the Fe-containing particles was produced via photochemical and/or aqueous oxidation over East Asia (Sullivan and Prather, 2007; Yang et al., 2009; Cheng et al., 2017).

The above observations about atmospheric processes of the Fe-containing particles were mainly performed in environments with low aerosol liquid water content. Cloud processing accompanied by high amounts of water played a vital role in the formation of secondary species (e.g., sulfate, nitrate, chloride, ammonium, and oxalate) through the partitioning of gas into aqueous phases or heterogeneous/multiphase processes (Sellegri et al. 2003; Lim et al., 2010; Chang et al., 2011; Harris et al., 2013). For example, one model study had estimated that up to 80 % of the total production of sulfate globally originated from aqueous reactions (Tsai et al., 2010). The presence of Fe in cloud droplets also allowed the conversion of SO_2 to sulfate via Fe-catalyzed autoxidation reactions (Harris et al., 2013). Furthermore, Fe chemistry involved in Fenton or Fenton-like reactions in cloud droplets yielded OH radicals that can induce the conversion of glyoxylic acid to low-volatility organic aerosols (e.g., oxalate) (Ervens et al., 2011). Various Fe-containing particle sources (such as dust and anthropogenic sources) might have different effects on the in-cloud formation of secondary species due to their different physicochemical properties (e.g., alkalinity) of these sources (Deguillaume et al., 2005). However, the effects of cloud processing on the formation of secondary species in various Fe-containing particle types remain poorly understood.

We have previously used a ground-based counterflow virtual impactor (GCVI) combined and a real-time single-particle aerosol mass spectrometer (SPAMS) to characterize chemical composition or the mixing state of cloud residues (Lin et al., 2017), the mixing state and cloud scavenging of the EC-containing particles (Zhang et al., 2017a), and the in-cloud formation of oxalate (Zhang et al., 2017b) at a mountain site in southern China. In this study, the same combined technology was utilized to obtain information on the characteristics and potential sources of Fe-containing cloud residues. Additionally, Fe-containing interstitial (non-activated particles) and cloud-free particles were also analyzed. The impact of cloud processing on the formation of sulfate, nitrate, chloride, ammonium, oxalate precursors, and oxalate in various Fe-containing particle types was addressed.

2 Experimental section

2.1 Sampling site

The sampling site was situated at the Nanling Background Station (112°53′56″ E, 24°41′56″ N; 1690 m a.s.l.) in southern China. The sampling site was in an acid precipitation region (Annual Environment Report of China in 2016, http://www.mee.gov.cn/hjzl/, last access: 28 January 2019). Due to the site being surrounded by a national park forest (273 km^2), it was minimally affected by local anthropogenic activities. However, it might be subjected to polluted air masses from the southern Pearl River Delta city groups or from northern China (Lin et al., 2017). A detailed description of the sampling site can be found elsewhere (Lin et al., 2017). The measurement campaign was conducted from 9 October to 4 November 2016. The time for cloud events was approximately 300 h in the whole period. The ambient temperature varied from 4 to 21 °C in this study (Fig. S1 in the Supplement), indicative of liquid-only clouds.

2.2 Instrumentation

Previous field measurement observed that the median size of cloud/fog droplets was approximately 10 µm in the study region (Wu et al., 2004). Cloud droplets with an aerodynamics diameter greater than 8 µm were collected using a GCVI inlet system (GCVI Model 1205, Brechtel Manufacturing Inc.). The collected cloud droplets were dried using an evaporation chamber (airflow temperature at 40 °C) in the GCVI until only dry residual particles (cloud residues) remained. To reliably guarantee the presence of cloud events, an upper-limit visibility threshold of 5 km and a lower-limit relative humidity (RH) threshold of 95 % were set in the GCVI software (Bi et al., 2016; Lin et al., 2017). During precipitation periods, the GCVI automatically shut down to protect

against interference from raindrops. The particle transmission efficiency of the cut size (8 µm) was 50 % (Shingler et al., 2012). Due to the cloud droplets being concentrated in the GCVI inlet, an enrichment factor was estimated to be 5.25 based on theoretical calculations (Shingler et al., 2012). More detailed information about the GCVI is given in Bi et al. (2016). The number concentration of particles collected by the GCVI was below 1 cm^3 during cloud-free periods, suggesting that instances of particle breakthrough and small particle contamination were absent (Shingler et al., 2012). In addition, interstitial particles were sampled using an inlet cyclone with a cut-off aerodynamic diameter of 2.5 µm ($PM_{2.5}$ inlet) during cloudy episodes. The cloud residues had also been observed to be larger in size relative to the interstitial particles (Fig. S2). Thus, it was proposed that the interstitial particles had not already proceeded to becoming cloud droplets. During cloud-free episodes, the $PM_{2.5}$ inlet was used to collect cloud-free particles. The measurement period of cloud residues, interstitial particles, and cloud-free particles are shown in Fig. S1.

The sampled cloud residues, interstitial particles, and cloud-free particles were subsequently measured by a single particle aerosol mass spectrometer (SPAMS) (Hexin Analytical Instrument Co., Ltd., Guangzhou, China) to obtain their size-resolved chemical composition. Bipolar mass spectra of individual aerosol particles were obtained by the SPAMS. The analytical method of the SPAMS has been described in Li et al. (2011). Briefly, the aerosol particles are focused into a narrow particle beam and accelerated to a region where the vacuum aerodynamic (d_{va}) size of the aerosol particles is measured using two continuous diode Nd : YAG laser beams (532 nm). Based on the calculated velocity of the particles, a pulsed high power laser (266 nm) can be precisely triggered to evaporate and ionize the particles. The production of positive and negative ions is subsequently recorded using a dual-polarity time-of-flight mass spectrometer. A specific mass-to-charge ratio (m/z) in the positive or negative mass spectrum can correspond to the most probable chemical species dependent on prior field and lab studies. The peak area of a specific m/z on individual particle is relevant to the mass of the corresponding chemical species (Bhave et al., 2002; Pratt et al., 2011). Polystyrene latex spheres (Nanosphere Size Standards, Duke Scientific Corp., Palo Alto) of 0.2–2.0 µm in diameter were used to calibrate the sizes of the detected particles at the sampling site. It should be noted that particles detected by the SPAMS are mostly distributed in the size range of d_{va} 0.2–2.0 µm (Li et al., 2011).

2.3 Screening of the Fe-containing aerosols

During the sampling period, 154 862 cloud residues, 15 420 interstitial particles, and 168 427 cloud-free particles with d_{va} ranging between 0.2 and 2.0 µm were chemically analyzed with the SPAMS. The Fe-containing aerosols typically had a positive ion peak at m/z 56. Since other species, such as $[CaO]^+$, $[KOH]^+$, and $[C_3H_4O]^+$, may also contribute to m/z 56, the natural isotopic composition of Fe ion peaks at both m/z 54 and 56 was chosen to strengthen the screening through excluding more ambiguous assignments (Zhang et al., 2014; Dall'Osto et al., 2016). Furthermore, the known isotopic ratio of Fe ($^{56}Fe/^{54}Fe = 16$) was used as an indicator for Fe (Beard and Johnson, 1999). The ratio to identify the Fe-containing particles might be below 16, due to organic peaks at m/z 54 and 56 in the Fe-containing particles. Considering the varied ratio resulting from the matrix effect of laser desorption/ionization (Allen et al., 2000), Furutani et al. (2011) performed a peak area ratio of m/z 56 to 54 above 3 to identify the Fe-containing particles. However, the average single-particle mass spectra with a ratio of m/z 56 to 54 below 10 can also be obtained in the organic carbon particles (Zhang et al., 2014). A high peak area ratio of m/z 56 to 54 above 10 was used in the present study, which had been applied in the previous studies (Zhang et al., 2014; Dall'Osto et al., 2016) to minimize the interference from other species. Thus, the Fe-containing particles in the study were identified by the coexistence of peaks at m/z 56 and m/z 54 and a peak area ratio ($^{56}Fe/^{54}Fe$) above 10. The errors were calculated assuming Poisson statistics for the analyzed particles in this work. A total of 5682 cloud droplet residues, 395 interstitial particles, and 5086 cloud-free particles were found to be internally mixed with Fe, representing 3.7 ± 0.1 % (by number), 2.6 ± 0.1 %, and 3.0 ± 0.1 % of the total measured cloud residues, interstitial particles, and cloud-free particles, respectively. Because the low number of the collected Fe-containing cloud residues limited the statistical analysis, the differences between single cloud events were not analyzed. Instead, an average analysis covering all the cloud events is presented.

The Fe-containing aerosols, including cloud residues, interstitial particles, and cloud-free particles, were initially grouped into 106 clusters using an adaptive resonance theory-based neural network algorithm (ART-2a) with a vigilance factor of 0.8, a learning rate of 0.05, and 20 iterations (Song et al., 1999). Then, by manually combining similar clusters, four primary types of Fe-containing aerosols were obtained, including Fe-rich, Fe internally mixed with mineral dust species (Fe-dust), Fe internally mixed with EC (Fe-EC), and Fe internally mixed with V (Fe-V).

3 Result and discussion

3.1 Characteristics and potential sources of the Fe-containing particle types

The averaged single-particle mass spectra of the four Fe-containing types are shown in Fig. 1. One common feature was that the four Fe-containing particle types were internally mixed with secondary inorganic ions such as sulfate (m/z −97 $[HSO_4]^-$) and/or nitrate (m/z −46 $[NO_2]^-$ or

$-62[NO_3]^-$). This suggests that the Fe-containing aerosols experienced atmospheric aging processes during long-range transport.

The Fe-rich type exhibited the highest peak at m/z 56 Fe as well as sulfate and nitrate, which was the largest fraction of Fe-containing particles, and contributed 84 ± 1 % (by number), 78 ± 4 %, and 81 ± 1 % to the Fe-containing cloud residues, interstitial particles, and cloud-free particles, respectively (Fig. 2). The crustal elements were rarely detected in the Fe-rich type, suggesting a non-mineral dust source. The Fe-rich type was unlikely to be caused by biomass burning sources due to the weak potassium (m/z 39 $[K]^+$) peak (Bi et al., 2011). Lithium (m/z 7 $[Li]^+$) was found to account for 7 ± 1 % (by number) of the Fe-rich type, implying a partial contribution from fly ash as suggested by Furutani et al. (2011). Zhang et al. (2014) considered that the Fe-rich particles were mostly produced by the iron/steel industry from Shanghai in eastern China. In this study, a steel production site with an annual yield of 6.5 million tons was located approximately 60 km east of the sampling site. The Fe-rich type detected here was most likely from industrial activities.

The Fe-dust type was mainly composed of mineral dust peaks including $[Al]^+$ (m/z 27), $[Ca]^+$ (m/z 40), $[SiO_3]^-$ (m/z −76), and $[PO_3]^-$ (m/z −79) (Fig. 1), which accounted for 12 ± 1 % (by number), 15 ± 2 %, and 12 ± 1 % of the Fe-containing cloud residues, interstitial particles, and cloud-free particles, respectively (Fig. 2). However, no clear enhanced number fraction (NF) of the Fe-dust type was detected in the particle size range of 1.0–2.0 µm relative to 0.2–1.0 µm (14 ± 1 % versus 12 ± 2 %, by number) (Fig. S3). The large Fe-dust particles (above 2.0 µm) might have already been deposited during transport. In addition, the Fe-dust particles may have a larger size (above 2.0 µm) that could not be detected by the SPAMS.

The Fe-EC type was characterized by EC cluster ions (e.g., m/z ±12 $[C]^{+/-}$, ±24 $[C_2]^{+/-}$, ±36 $[C_3]^{+/-}$, ±48 $[C_4]^{+/-}$, ±60 $[C_5]^{+/-}$) as well as strong sulfate (Fig. 1). The internal mixture of Fe-containing particles with EC was also observed in the Asian outflow atmosphere, mainly due to the contribution from fossil fuel combustion in China (Furutani et al., 2011). The Fe-V type showed the intense $[Fe]^+$ and $[V]^+$ (m/z 51) or vanadium oxide (m/z 67$[VO]^+$) peaks (Fig. 1). The Fe-V type was possibly related to residual fuel oil combustion sources, such as ships and refineries (Furutani et al., 2011; Zhang et al., 2014; Dall'Osto et al., 2016). The Fe-EC and Fe-V types were minor contributors (below 5 ± 1 %, by number) in this study (Fig. 2).

3.2 The impact of cloud processing on secondary inorganic species in the Fe-containing cloud residues

Sulfate, nitrate, chloride, and ammonium were the most common secondary inorganic species produced by aqueous reactions. Comparisons of these secondary inorganic species between Fe-containing cloud residues, interstitial particles and cloud-free particles showed the impact of cloud processing or aqueous phases on the formation of these species associated with Fe-containing particles. Comparisons during daytime (local time 08:00–20:00) and nighttime (local time 20:00–08:00) were also performed to investigate the irradiation effect. The ambient temperature showed a typically diurnal pattern. However, RH had a high value (nearly 100 %) during daytime when the cloud events exited. Note that variation in the meteorological conditions may influence the comparisons. Due to the low number of particles detected, the Fe-EC and Fe-V particle types were not analyzed in this section.

The NFs of sulfate in the Fe-containing cloud residues (93 ± 1 %, by number) and interstitial particles (92 ± 4 %) were similar to those in the cloud-free particles (96 ± 1 %), as shown in Fig. 3. The NFs of sulfate in the non-Fe cloud residues and interstitial particles were also not observed to be enhanced relative to the non-Fe cloud-free particles (87 ± 1 % and 88 ± 1 % versus 92 ± 1 %, by number). Several field studies also failed to find the increased NF or mass fraction of sulfate in cloud residues or interstitial particles (Drewnick et al., 2007; Twohy and Anderson, 2008; Schneider et al., 2017). The cause for these observations remained unknown. In this study, an extremely high NF (above 90 %) of sulfate was measured in the Fe-containing cloud-free particles, which makes it hard to find the minor changes after the particles experienced cloud events. It was worth noting that the Fe-containing particles might experience one or more cloud processes prior to arrival at the observed site, wherein sulfate may have accumulated on the Fe-containing particles. A low SO_2 level (below 5 ppb) in the observed site may also limit the formation of sulfate. Thus, we speculated that the contribution from the in-cloud formation of sulfate was relatively small compared to the total amount of sulfate in the Fe-containing cloud-free particles in this study.

The NFs of nitrate in the Fe-containing cloud residues (86 ± 1 %, by number) and interstitial particles (89 ± 5 %) were enhanced in comparison to the cloud-free particles (76 ± 1 %) (Fig. 3). The enhanced NF of nitrate during cloud processing can be attributed to the partitioning from gaseous HNO_3 into the aqueous phase and/or the heterogeneous reaction of N_2O_5 (Hayden et al., 2008; Chang et al., 2011; Schneider et al., 2017). Photochemical reactions probably played a vital role in nitrate formation (Pathak et al., 2009), leading to the increased NF of nitrate in the Fe-containing cloud-free particles during daytime (Fig. 4b). However, in the case of the Fe-containing cloud residues, there was no distinct change in the NF of nitrate between daytime and nighttime (Fig. 4b), reflecting that the in-cloud formation of nitrate was less affected by photochemical reactions. The NF of nitrate in the Fe-dust cloud residues was higher than that in the Fe-rich cloud residues (92 ± 3 % versus 86 ± 1 %, by number), despite a similar NF of nitrate observed in the two Fe-containing cloud-free particle types (Fig. 4b). This can be

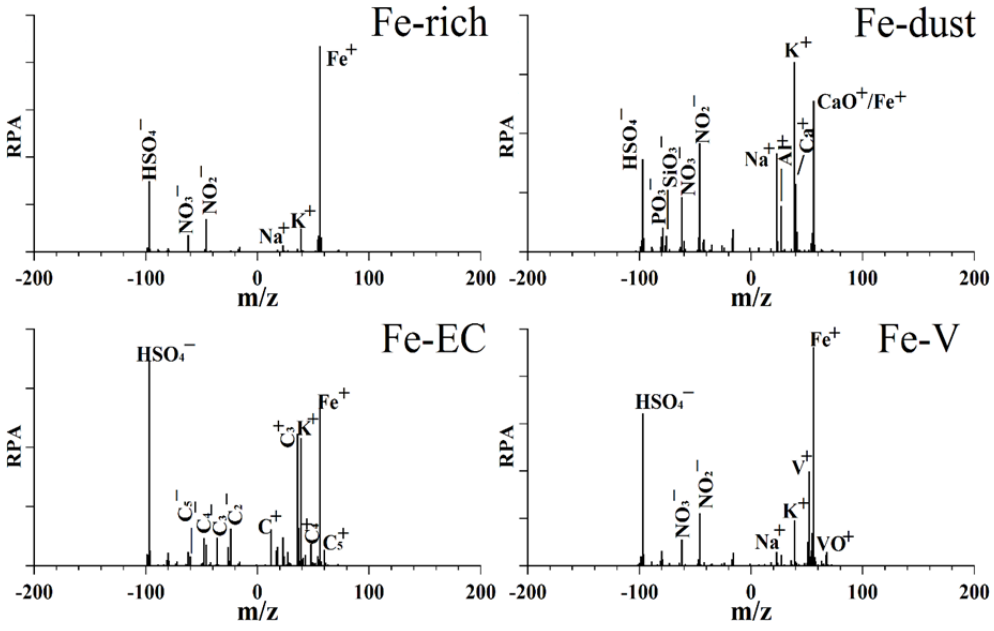

Figure 1. The average single-particle mass spectra of the four Fe-containing types. RPA refers to relative peak area.

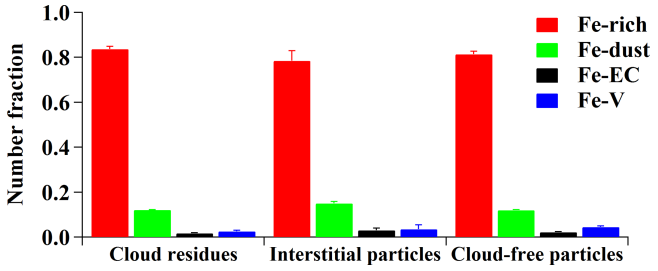

Figure 2. Number fraction of the four Fe-containing types in the Fe-containing cloud residues, interstitial particles, and cloud-free particles during the whole study period.

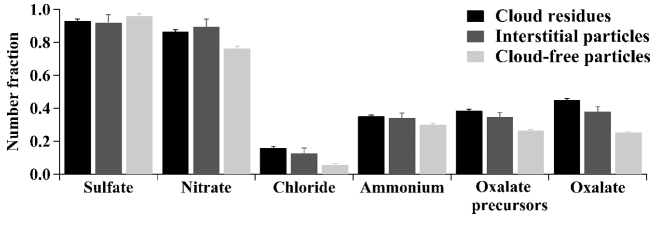

Figure 3. Comparison in number fractions of sulfate (m/z −97), nitrate (m/z −46 or −62), chloride (m/z −35 or −37), ammonium (m/z 18), oxalate precursors (m/z −59, −71, −73, −87, −103, or −117), and oxalate (m/z −89) between the Fe-containing cloud residues, interstitial particles, and cloud-free particles.

explained by the fact that gaseous HNO_3 would be neutralized upon reaction with alkaline-rich (e.g., Ca) particles in the Fe-dust cloud residues during cloud processing (Matsuki et al., 2010).

Higher NFs of chloride were found in the Fe-containing cloud residues and interstitial particles compared to the cloud-free particles (16 ± 1 % or 13 ± 2 % versus 6 ± 1 %, by number) (Fig. 3). The partitioning of volatile gaseous chloride (i.e., HCl) into the aqueous phase was a major contributor to the increased chloride in cloud droplets (Sellegri et al., 2003). The enhanced NF of chloride during cloud processing was unlikely to have resulted from the invasion of sea salt particles because 0.40 ± 0.01 % (by number) of the Fe-containing cloud residues was found to internally mix with the related sea salt peaks (e.g., m/z 81 $[Na_2^{35}Cl]^+$ or 83 $[Na_2^{37}Cl]^+$). Only 115 sea salt particles were obtained in the non-Fe cloud residues, suggesting less gaseous HCl was released from aged sea salt particles during cloud processing. Recently, Fu et al. (2018) reported that the anthropogenic gaseous HCl emission was estimated to be in the range of 20–200 kg km^{-2} in southern China, mostly from coal burning, agricultural biomass burning, and waste incineration. The gaseous HCl sources in this region might originate from regional transport of this anthropogenic HCl in southern China. The irradiation effect during daytime would generally result in the reduction of ammonium chloride in the particles due to evaporation at high temperature (Huang et al., 2011). In this study, there was no change in NF of chloride in the Fe-containing cloud residues between daytime and nighttime (Fig. 4c), suggesting that the amount of in-cloud chloride formation was less affected by irradiation effect. In the case of cloud-free events, no decreased NF of chloride in the Fe-containing cloud-free particles was also observed during daytime relative to the nighttime (Fig. 4c), presumably due to the formation of calcium chloride (Sullivan et al.,

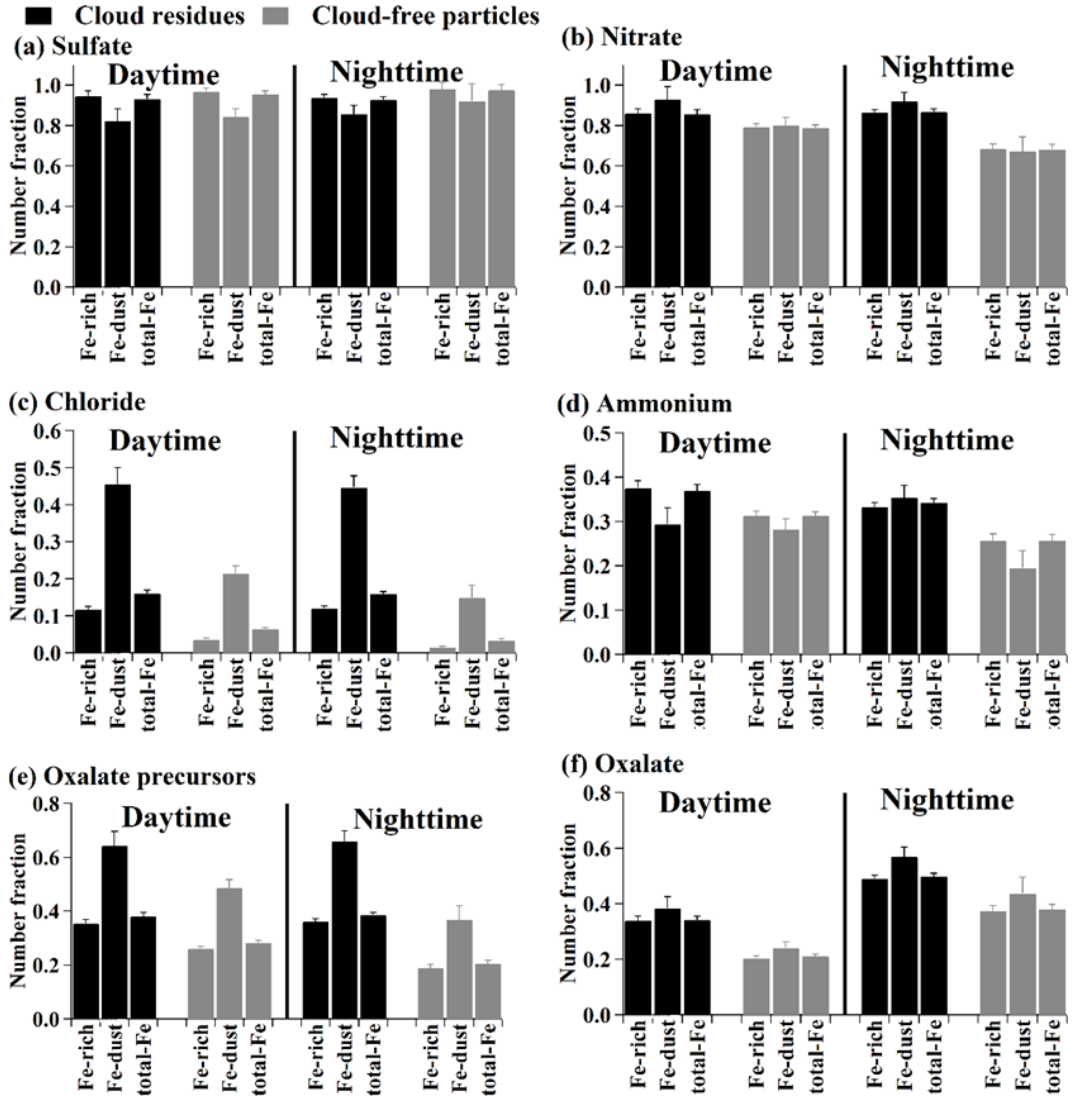

Figure 4. Comparison in number fractions of sulfate (m/z −97), nitrate (m/z −46 or −62) , chloride (m/z −35 or −37), ammonium (m/z 18), oxalate precursors (m/z −59, −71, −73, −87, −103, or −117), and oxalate (m/z −89) in the Fe-rich, Fe-dust, and all Fe-containing (total-Fe) types between the cloud residues and cloud-free particles types and their difference during daytime and nighttime. The comparison was not performed for the interstitial particles due to the low number of detected particles.

2007b). A significant feature was also found in that the NF of chloride in the Fe-dust cloud residues was much higher than that in the Fe-rich cloud residues (45 ± 3 % versus 12 ± 1 %, by number) (Fig. 4c). Relative to sulfate and nitrate, chloride showed a highly internally mixed state with Ca particles (Fig. S4), indicating that the Ca-rich particles in the Fe-dust cloud residues were responsible for the in-cloud formation of chloride. Despite lower amounts (13 ± 1 %, by number) of Ca particles in the Fe-rich cloud residues, the enhanced NF of chloride was obvious (Fig. 4c). This was likely attributed to the uptake of volatile gaseous chloride (i.e., HCl) over simple physical sorption due to the high water solubility of gaseous HCl (Sellegri et al., 2003).

The NFs of ammonium in the Fe-containing cloud residues (35 ± 1 %, by number) and interstitial particles (34 ± 3 %) were analogous to those in the cloud-free particles (30 ± 1 %) (Fig. 3). During nighttime, the significantly increased NF of ammonium in the Fe-containing cloud residues was observed as compared to the cloud-free particles, especially for the Fe-dust type (35 ± 1 % versus 20 ± 1 %, by number) (Fig. 4d). Most ammonium in the Fe-dust cloud residues was internally mixed with sulfate and/or nitrate. The secondary acids accumulated on the Fe-Dust cloud residues might be a sink for NH_3 (Sullivan et al., 2007a; Nie et al., 2012). During daytime, the increased NF of ammonium in the Fe-dust cloud-free particles was likely attributed to the enhanced NF of ammonium nitrate. This process might lead to a minor change

in the NF of ammonium between the Fe-dust cloud residues and cloud-free particles during daytime.

3.3 The impact of cloud processing on oxalate precursors and oxalate in the Fe-containing cloud residues

The aqueous oxidation pathway of organic precursors was an important contributor to the in-cloud formation of oxalate (Sorooshian et al., 2007; Zhang et al., 2017b). Acetate (at m/z −59 $[C_2H_3O_2]^-$), methylglyoxal (m/z −71 $[C_3H_3O_2]^-$), glyoxylate (m/z −73 $[C_2HO_3]^-$), pyruvate (m/z −87 $[C_3H_3O_3]^-$), malonate (m/z −103 $[C_3H_3O_4]^-$), and succinate (m/z −117 $[C_4H_5O_4]^-$) had been suggested as the main precursors for the formation of oxalate in the atmospheric aqueous phase (Ervens et al., 2004; Lim et al., 2005; Sorooshian et al., 2006). A peak at m/z −59 might also originate from the presence of $[HCNO_2]^-$ or levoglucosan (Bi et al., 2011). Increased NFs of the precursors were clearly identified in the Fe-containing cloud residues (38 ± 1 %, by number) and interstitial particles (35 ± 3 %) compared to cloud-free particles (26 ± 1 %) (Fig. 3). These findings indicate the contribution of cloud processing to the formation of oxalate precursors. Photochemical reactions were another major pathway to form oxalate precursors (Kawamura and Bikkina, 2016). Although enhanced NF of the oxalate precursors was observed in the Fe-containing cloud-free particles during daytime, no variation in NF of the oxalate precursors was found in the Fe-containing cloud residues during either daytime or nighttime (Fig. 4e). Therefore, the in-cloud formation of the oxalate precursors is less likely to be influenced by photochemical reactions. Interestingly, these precursors presented in 62 ± 2 % (by number) of the Fe-dust cloud residues, which was much higher than 35 ± 1 % (by number) of the Fe-rich cloud residues (Fig. 4e). A similar trend was also found during the cloud-free periods (43 ± 2 % versus 23 ± 1 %, by number) (Fig. 4e). These findings suggest that the oxalate precursors would readily become enriched in the Fe-dust particles.

The NFs of oxalate in the Fe-containing cloud residues (45 ± 1 %, by number) and interstitial particles (38 ± 3 %) were higher than that in the cloud-free particles (26 ± 1 %) (Fig. 3). Enhanced NFs of oxalate without its precursors were found for the Fe-containing cloud residues (15 ± 1 %, by number) and interstitial particles (13 ± 2 %) in comparison to the cloud-free particles (10 ± 1 %) (Fig. S5). This possibly resulted from gaseous oxalic acid partitioning into cloud droplets (Sellegri et al., 2003). It should be mentioned here that such an enhancement of oxalate may be related to other precursors (e.g., glutarate) that were not considered in this study. On the other hand, oxalate that was internally mixed with its precursors accounted for 30 ± 1 % (by number) and 25 ± 2 % of the Fe-containing cloud residues and interstitial particles, respectively, which were much higher than the amount in the cloud-free particles (16 ± 1 %) (Fig. S5). This result indicates that the presence of oxalate precursors would enhance the in-cloud formation of oxalate, mostly via the aqueous oxidation of oxalate precursors (Ervens et al., 2004; Sorooshian et al., 2006). Compared with the Fe-rich cloud residues, the higher NF of oxalate in the Fe-dust cloud residues (Fig. 4f) might be related to the plentiful precursors in the Fe-dust cloud residues (Fig. 4e). A lower NF of oxalate in the Fe-containing cloud residues was measured during daytime relative to nighttime, indicating the photolysis of Fe-oxalate complexes (Fig. 4f). This phenomenon differed greatly from the in-cloud formation of nitrate, chloride, and oxalate precursors in that their NF had no obvious change during both daytime and nighttime. The lower NF of oxalate in the Fe-containing cloud residues during daytime also implies that the photolysis of Fe-oxalate complexes could overwhelm the in-cloud formation of oxalate during the day.

The Fenton reaction ($Fe^{2+} + H_2O_2 \rightarrow Fe^{3+} + OH^- + \cdot OH$) would yield OH radicals, which promote the conversion of the precursors to oxalate during cloud processing (Lim et al., 2010). Higher NF of oxalate in the Fe-containing cloud residues was compared with the non-Fe cloud residues (45 ± 1 % versus 7 ± 1 %, by number) (Fig. S6). Moreover, a peak area ratio of oxalate to its precursors was enhanced in the Fe-containing cloud residues relative to non-Fe cloud residues (Fig. 5a). These findings imply that aqueous-phase OH was likely produced by redox cycling of the Fe-driven Fenton reaction (Hems et al., 2017) and thus enhanced the oxidation of various precursors to form oxalate during cloud processing. Sorooshian et al. (2007) observed that oxalate was more efficiently produced from aqueous oxidation of glyoxylate with higher cloud liquid water content, corresponding to higher cloud droplet pH values. Relative to Fe-containing interstitial particles, an increased peak area ratio of oxalate to its precursors in the cloud residues (Fig. 5a) might be due to their higher liquid water content. Moreover, in the presence of ammonium, the peak area ratio of oxalate to its precursors was also enhanced in the Fe-containing cloud residues (Fig. S7). The enhanced peak area ratio of oxalate to its precursors in the Fe-dust cloud residues at night was likely due to the enhancement of ammonium (Fig. 5b). Furthermore, nearly 90 ± 3 % (by number) of oxalate in the Fe-dust cloud residues was found to be internally mixed with ammonium during nighttime. Ortiz-Montalvo et al. (2013) considered that the formation of ammonium oxalate would substantially reduce the vapor pressure of oxalate, enhancing the yield of oxalate during cloud processing. During the daytime, the decreased peak area ratio of oxalate to its precursors mostly resulted from the degradation of oxalate associated with the photolysis of Fe-oxalate complexes.

3.4 Mixing state of the Fe-containing cloud residues

Figure 6 displays the NF of various species in the four Fe-containing cloud residual types. Abundant sulfate was found in the Fe-rich (94 ± 1 %, by number), Fe-dust (85 ± 4 %), Fe-

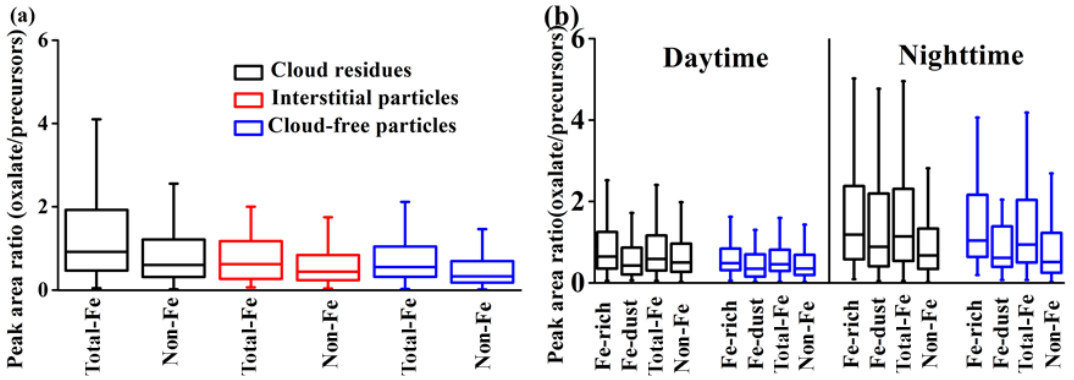

Figure 5. Peak area ratio of oxalate (m/z −89) to the sum of the peak areas of its precursors (m/z −59, −71, −73, −87, −103, or −117) in the total-Fe and non-Fe types **(a)**. Peak area ratio of oxalate to its precursors in the Fe-rich, Fe-dust, total-Fe, and non-Fe types during daytime and nighttime **(b)**.

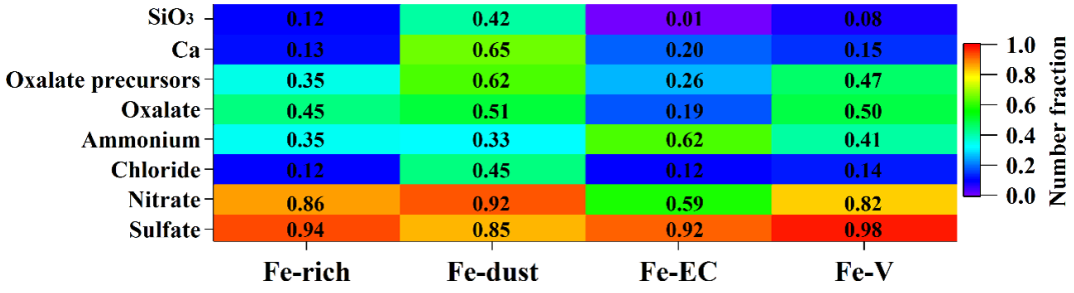

Figure 6. The number fractions of sulfate (m/z −97), nitrate (m/z −46 or −62), chloride (m/z −35 or −37), ammonium (m/z 18), oxalate (m/z −89), oxalate precursors (m/z −59 , −71, −73, −87, 103, or −117), Ca (m/z 40), and $[SiO_3]^-$ (m/z -76) in the four Fe-containing cloud residues.

EC (92 ± 10 %), and Fe-V (98 ± 8 %) cloud residues. Substantial sulfate in the Fe-containing particles was also observed over East Asia (Furutani et al., 2011; Moffet et al., 2012; Li et al., 2013). Despite no significantly increased NF of sulfate in Fe-containing particles during cloud processing, the substantial sulfate observed here was expected due to the likely high levels of SO_2 encountered during long-distance transport. High amounts (above 80 %, by number) of nitrate were observed in the Fe-containing cloud residues except for the Fe-EC type (59 ± 8 %). However, a relatively high NF of ammonium was obtained in the Fe-EC cloud residues (62 ± 8 %, by number) compared to the other Fe-containing cloud residual types (below 45 %). Approximately 97 ± 1 % (by number) and 54 ± 5 % of ammonium were internally mixed with sulfate and nitrate, respectively, in the Fe-EC type, suggesting that ammonium in the Fe-EC cloud residues has a greater contribution from ammonium sulfate rather than ammonium nitrate. It should be noted here that the evaporation chamber of the GCVI may lead to a depletion of ammonium nitrate in the Fe-EC cloud residues (Hayden et al., 2008). The higher NF of chloride was found in the Fe-dust cloud residues (45 ± 3 %, by number) relative to the other Fe-containing cloud residual types (below 15 %). As discussed above, the Ca-rich particles in the Fe-dust type contributed considerably to the in-cloud formation of chloride. Oxalate accounted for 45 ± 1 % (by number), 51 ± 3 %, and 50 ± 6 % of the Fe-rich, Fe-dust, and Fe-V cloud residues, respectively, which was much higher than the oxalate found in Fe-EC cloud residues (19 ± 4 %). The lower NF of oxalate in the Fe-EC cloud residues might be restricted by the low NF of the oxalate precursors.

4 Conclusions and atmospheric implications

Previous laboratory and modeling studies focused on the cloud processing of Fe-containing particles from dust sources (Hand et al., 2004; Mahowald et al., 2005; Shi et al., 2009). Several modeling and field studies argued that the combustion Fe sources should be taken into account over East Asia (Luo et al., 2008; Furutani et al., 2011; Moffet et al., 2012; Zhang et al., 2014; Ito, 2015). This study includes the first report of the abundant Fe-rich particles related to the participation of combustion sources in cloud processing over East Asia.

Luo et al. (2008) performed a modeling calculation to estimate the influence of atmospheric process on soluble Fe by assuming that cloud processing had sufficient acidic species

to process more soluble Fe. However, they did not definite the specific acid types. In the current study, the enhanced NFs of nitrate and chloride in the Fe-containing particles was produced via partitioning and the heterogeneous/aqueous chemistry of gaseous HNO_3 and HCl or other precursors. More importantly, the in-cloud formation of nitrate and chloride was enhanced in the Fe-dust type relative to the Fe-rich type. Laboratory studies also showed that Fe dissolution in the HCl solution differed from that in the H_2SO_4 and HNO_3 solutions (Fu et al., 2010; Rubasinghege et al., 2010). In order to accurately predict bioavailable Fe during cloud processing, the impact of different acids on Fe dissolution in varied Fe types might be considered for future modeling study.

Modeling calculations showed that relative to proton-promoted Fe dissolution, the addition of oxalate accompanied by the photolysis of Fe-oxalate complexes in aqueous chemistry more than doubled the soluble Fe deposition from combustion sources in global oceanic regions (Ito, 2015). Our data showed that aqueous-phase oxidation of the oxalate precursors was an important contributor to the in-cloud formation of oxalate in the Fe-rich particles. The Fe-driven Fenton reaction likely accelerates the conversion of the oxalate precursors to oxalate in the Fe-rich particles during cloud processing. Moreover, the complexation of Fe with oxalate might further increase oxalate content in the Fe-rich cloud residues (Chen and Grassian, 2013). Ammonium species possibly enhance the oxidation of precursors to form oxalate in the Fe-rich cloud residues through increasing aerosol pH. On the other hand, the photolysis of Fe-oxalate complexes in the Fe-rich cloud residues would lead to the losses of oxalate during daytime. These results supported the role of oxalate in aqueous chemistry in soluble Fe deposition from combustion sources. However, the modeling study assumed that oxalate entirely mixed with Fe-containing particles from combustion sources in the bulk aqueous phase (Ito, 2015). In this work, nearly 45 ± 1 % (by number) of the Fe-rich cloud residues contained only oxalate. The mass concentration of oxalate in the bulk aqueous phase might be overestimated in model simulations. This might suppress Fe dissolution under a low concentration of oxalate because of competition of oxalate complexation between dissolved Fe in solution and Fe on the particle surface (Chen and Grassian, 2013).

Data availability. All the data can be obtained by contacting the corresponding author Xinhui Bi (bixh@gig.ac.cn).

Supplement. The supplement related to this article is available online at: https://doi.org/10.5194/acp-19-1195-2019-supplement.

Author contributions. XHB, GHZ, and QHL planned and designed the experimental setup. YXY, LP, XFL, YZF, and JO performed the atmospheric measurement and collected the data. QHL and XHB analyzed the data and wrote the manuscript. ML, DHC, MM, MJT, XMW, PAP, GYS, and ZZ contributed comments.

Competing interests. The authors declare that they have no conflict of interest.

Acknowledgements. This work was supported by the National Key Research and Development Program of China (2017YFC0210104), the National Nature Science Foundation of China (no. 41877307, 41775124 and 41805103), the Foundation for Leading Talents of the Guangdong Province Government, and the State Key Laboratory of Organic Geochemistry (SKLOG2016-A05). Mingjin J. Tang would like to thank the Chinese Academy of Sciences international collaborative project (no. 132744KYSB20160036). This is contribution no.IS-2641 from GIGCAS.

Edited by: Yves Balkanski
Reviewed by: three anonymous referees

References

Abbaspour, N., Hurrell, R., and Kelishadi, R.: Review on iron and its importance for human health, J. Res. Med. Sci., 19, 164–174, 2014.

Allen, J. O., Fergenson, D. P., Gard, E. E., Hughes, L. S., Morrical, B. D., Kleeman, M. J., Gross, D. S., Galli, M. E., Prather, K. A., and Cass, G. R.: Particle detection efficiencies of aerosol time of flight mass spectrometers under ambient sampling conditions, Environ. Sci. Technol., 34, 211–217, https://doi.org/10.1021/es9904179, 2000.

Beard, B. L. and Johnson, C. M.: High precision iron isotope measurements of terrestrial and lunar materials, Geochim. Cosmochim. Ac., 63, 1653–1660, https://doi.org/10.1016/S0012-821X(01)00581-7, 1999.

Bhave, P. V., Allen, J. O., Morrcal, B. D., Fergenson, D. P., Cass, G. R., and Prather, K. A.: A field-based approach for determining atofms instrument sensitivities to ammonium and nitrate, Environ. Sci. Technol., 36, 4868–4879, https://doi.org/10.1021/es015823i, 2002.

Bi, X., Zhang, G., Li, L., Wang, X., Li, M., Sheng, G., Fu, J., and Zhou, Z.: Mixing state of biomass burning particles by single particle aerosol mass spectrometer in the urban area of PRD, China, Atmos. Environ., 45, 3447–3453, https://doi.org/10.1016/j.atmosenv.2011.03.034, 2011.

Bi, X., Lin, Q., Peng, L., Zhang, G., Wang, X., Brechtel, F. J., Chen, D., Li, M., Peng, P. A., Sheng, G., and Zhou, Z.: In situ detection of the chemistry of individual fog droplet residues in the Pearl River Delta region, China, J. Geophys. Res.-Atmos., 121, 9105–9116, https://doi.org/10.1002/2016JD024886, 2016.

Chang, W. L., Bhave, P. V., Brown, S. S., Riemer, N., Stutz, J., and Dabdub, D.: Heterogeneous atmospheric chemistry, ambient measurements, and model calculations of N_2O_5: A review, Aerosol Sci. Tech., 45, 665–695, https://doi.org/10.1080/02786826.2010.551672, 2011.

Chen, H. and Grassian, V. H.: Iron dissolution of dust source materials during simulated acidic processing: The effect of sulfuric, as-

cetic, and oxalic acids, Environ. Sci. Technol., 47, 10312–10321, https://doi.org/10.1021/es401285s, 2013.

Cheng, C., Li, M., Chan, C.K., Tong, H., Chen, C., Chen, D., Wu, D., Li, L., Wu, C., Cheng, P., Gao, W., Huang, Z., Li, X., Zhang, Z., Fu, Z., Bi, Y., and Zhou, Z.: Mixing state of oxalic acid containing particles in the rural area of Pearl River Delta, China: implications for the formation mechanism of oxalic acid, Atmos. Chem. Phys., 17, 9519–9533, https://doi.org/10.5194/acp-17-9519-2017, 2017.

Costa, D. L. and Dreher, K. L.: Bioavailable transition metals in particulate matter mediate cardiopulmonary injury in healthy and compromised animalmodels, Environ. Health Persp., 105, 1053–1060, https://doi.org/10.1289/ehp.97105s51053, 1997.

Dall'Osto, M., Beddows, D. C., Harrison, R. M., and Onat, B.: Fine iron aerosols are internally mixed with nitrate in the urban European atmosphere, Environ. Sci. Technol., 50, 4212–4220, https://doi.org/10.1021/acs.est.6b01127, 2016.

Deguillaume, L., Leriche, M., Desboeufs, K., Mailhot, G., George, C., and Chaumerliac, N.: Transition metals in atmospheric liquid phases: Sources, reactivity, and sensitive parameters, Chem. Rev., 105, 3388–3431, https://doi.org/10.1021/cr040649c, 2005.

Drewnick, F., Schneider, J., Hings, S. S., Hock, N., Noone, K., Targino, A., Weimer, S., and Borrmann, S.: Measurement of ambient, interstitial, and residual aerosol particles on a mountaintop site in central Sweden using an aerosol mass spectrometer and a CVI, J. Atmos. Chem., 56, 1–20, https://doi.org/10.1007/s10874-006-9036-8, 2007.

Ervens, B., Feingold, G., Frost, G. J., and Kreidenweis, S. M.: A modeling study of aqueous production of dicarboxylic acids: 1. chemical pathways and speciated organic mass production, J. Geophys. Res.-Atmos., 109, D15205, https://doi.org/10.1029/2003JD004387, 2004.

Ervens, B., Turpin, B., and Weber, R.: Secondary organic aerosol formation in cloud droplets and aqueous particles (aqSOA): a review of laboratory, field and model studies, Atmos. Chem. Phys., 11, 11069–11102, https://doi.org/10.5194/acp-11-11069-2011, 2011.

Fomba, K.W., Müller, K., Van Pinxteren, D., and Herrmann, H.: Aerosol size-resolved trace metal composition in remote northern tropical Atlantic marine environment: case study Cape Verde islands, Atmos. Chem. Phys., 13, 4801–4814, https://doi.org/10.5194/acp-13-4801-2013, 2013.

Fu, H., Cwiertny, D. M., Carmichael, G. R., Scherer, M. M., and Grassian, V. H.: Photoreductive dissolution of Fe-containing mineral dust particles in acidic media, J. Geophys. Res.-Atmos., 115, D11304, https://doi.org/10.1029/2009JD012702, 2010.

Fu, X., Wang, T., Wang, S., Zhang, L., Cai, S., Xing, J., and Hao, J.: Anthropogenic emissions of hydrogen chloride and fine particulate chloride in China, Environ. Sci. Technol., 52, 1644–1654, https://doi.org/10.1021/acs.est.7b05030, 2018.

Furutani, H., Jung, J., Miura, K., Takami, A., Kato, S., Kajii, Y., and Uematsu, M.: Single-particle chemical characterization and source apportionment of iron-containing atmospheric aerosols in Asian outflow, J. Geophys. Res.-Atmos., 116, D18204, https://doi.org/10.1029/2011JD015867, 2011.

Hand, J. L., Mahowald, N. M., Chen, Y., Siefert, R. L., Luo, C., Subramaniam, A., and Fung, I.: Estimates of atmospheric-processed soluble iron from observations and a global mineral aerosol model: biogeochemical implications, J. Geophys. Res.-Atmos., 109, D17205, https://doi.org/10.1029/2004JD004574, 2004.

Harris, E., Sinha, B., van Pinxteren, D., Tilgner, A., Fomba, K. W., Schneider, J., Roth, A., Gnauk, T., Fahlbusch, B., Mertes, S., Lee, T., Collett, J., Foley, S., Borrmann, S., and Herrmann., H.: Enhanced role of transition metal ion catalysis during in-cloud oxidation of SO_2, Science, 340, 727–730, https://doi.org/10.1126/science.1230911, 2013.

Hayden, K. L., Macdonald, A. M., Gong, W., Toom-Sauntry, D., Anlauf, K. G., Leithead, A., Li, S. M., Leaitch, W. R., and Noone, K.: Cloud processing of nitrate, J. Geophys. Res.-Atmos., 113, D18201, https://doi.org/10.1029/2007JD009732, 2008.

Hems, R. F., Hsieh, J. S., Slodki, M. A., Zhou, S., and Abbatt, J. P.: Suppression of OH generation from the Photo-Fenton reaction in the presence of α-Pinene secondary organic aerosol material, Environ. Sci. Technol. Lett., 410, 439–443, https://doi.org/10.1021/acs.estlett.7b00381, 2017.

Huang, X. F., He, L. Y., Hu, M., Canagaratna, M. R., Kroll, J. H., Ng, N. L., Zhang, Y. H., Lin, Y., Xue, L., Sun, T. L., Liu, X. G., Shao, M., Jayne, J. T., and Worsnop, D. R.: Characterization of submicron aerosols at a rural site in Pearl River Delta of China using an Aerodyne High-Resolution Aerosol Mass Spectrometer, Atmos. Chem. Phys., 11, 1865–1877, https://doi.org/10.5194/acp-11-1865-2011, 2011.

Ito, A.: Atmospheric processing of combustion aerosols as a source of bioavailable iron, Environ. Sci. Technol. Lett., 2, 70–75, https://doi.org/10.1021/acs.estlett.5b00007, 2015.

Jickells, T. D., An, Z. S., Andersen, K. K., Baker, A. R., Bergametti, G., Brooks, N., Cao, J. J., Boyd, P. W., Duce, R. A., Hunter, K. A., Kawahata, H., Kubilay, N., LaRoche, J., Liss, P. S., Mahowald, N., Prospero, J. M., Ridgwell, A. J., Tegen, I., and Torres, R.: Global iron connections between desert dust, ocean biogeochemistry, and climate, Science, 308, 67–71, https://doi.org/10.1126/science.1105959, 2005.

Kawamura, K. and Bikkina, S.: A review of dicarboxylic acids and related compounds in atmospheric aerosols: molecular distributions, sources and transformation, Atmos. Res., 170, 140–160, https://doi.org/10.1016/j.atmosres.2015.11.018, 2016.

Li, L., Huang, Z., Dong, J., Li, M., Gao, W., Nian, H., Fu, Z., Zhang, G., Bi, X., and Cheng, P.: Real time bipolar time-of-flight mass spectrometer for analyzing single aerosol particles, Int. J. Mass Spectrom., 303, 118–124, https://doi.org/10.1016/j.ijms.2011.01.017, 2011.

Li, W., Wang, T., Zhou, S., Lee, S., Huang, Y., Gao, Y., and Wang, W.: Microscopic observation of metal-containing particles from Chinese continental outflow observed from a non-industrial site, Environ. Sci. Technol., 47, 9124–9131, https://doi.org/10.1021/es400109q, 2013.

Lim, H. J., Carlton, A. G., and Turpin, B. J.: Isoprene forms secondary organic aerosol through cloud processing: Model simulations, Environ. Sci. Technol., 39, 4441–4446, https://doi.org/10.1021/es048039h, 2005,

Lim, Y. B., Tan, Y., Perri, M. J., Seitzinger, S. P., and Turpin, B. J.: Aqueous chemistry and its role in secondary organic aerosol (SOA) formation, Atmos. Chem. Phys., 10, 10521–10539, https://doi.org/10.5194/acp-10-10521-2010, 2010.

Lin, Q., Zhang, G., Peng, L., Bi, X., Wang, X., Brechtel, F. J., Li, M., Chen, D., Peng, P., Sheng, G., and Zhou, Z.: In situ chemical composition measurement of individual cloud residue particles at

a mountain site, southern China, Atmos. Chem. Phys., 17, 8473–8488, https://doi.org/10.5194/acp-17-8473-2017, 2017.

Luo, C., Mahowald, N., Bond, T., Chuang, P. Y., Artaxo, P., Siefert, R., Chen, Y., and Schauer, J.: Combustion iron distribution and deposition, Global Biogeochem. Cy., 22, GB1012, https://doi.org/10.1029/2007GB002964, 2008.

Mahowald, N. M., Baker, A. R., Bergametti, G., Brooks, N., Duce, R. A., Jickells, T. ., Kubilay, N., Prospero, J. M., and Tegen, I.: Atmospheric global dust cycle and iron inputs to the ocean, Global Biogeochem. Cy., 19, GB4025, https://doi.org/10.1029/2004GB002402, 2005.

Matsuki, A., Schwarzenboeck, A., Venzac, H., Laj, P., Crumeyrolle, S., and Gomes, L.: Cloud processing of mineral dust: direct comparison of cloud residual and clear sky particles during AMMA aircraft campaign in summer 2006, Atmos. Chem. Phys., 10, 1057–1069, https://doi.org/10.5194/acp-10-1057-2010, 2010.

Moffet, R. C., Furutani, H., Rödel, T. C., Henn, T. R., Sprau, P. O., Laskin, A., Uematsu, M., and Gilles, M. K.: Iron speciation and mixing in single aerosol particles from the Asian continental outflow, J. Geophys. Res.-Atmos., 117, D07204, https://doi.org/10.1029/2011JD016746, 2012.

Nie, W., Wang, T., Xue, L. K., and Ding, A. J.: Asian dust storm observed at a rural mountain site in southern china: chemical evolution and heterogeneous photochemistry, Atmos. Chem. Phys., 12, 11985–11995, https://doi.org/10.5194/acp-12-11985-2012, 2012.

Ortiz-Montalvo, D. L., Häkkinen, S. A. K., Schwier, A. N., Yong, B. L., Mcneill, V. F., and Turpin, B. J.: Ammonium addition (and aerosol pH) has a dramatic impact on the volatility and yield of glyoxal secondary organic aerosol, Environ. Sci. Technol., 48, 255–262, https://doi.org/10.1021/es4035667, 2013.

Pathak, R. K., Wu, W. S., and Wang, T.: Summertime $PM_{2.5}$ ionic species in four major cities of china: nitrate formation in an ammonia-deficient atmosphere, Atmos. Chem. Phys., 9, 1711–1722, https://doi.org/10.5194/acp-9-1711-2009, 2009.

Pratt, K. A., Murphy, S. M., Subramanian, R., Demott, P. J., Kok, G. L., Campos, T., Rogers, D. C., Prenni, A. J., Heymsfield, A. J., Seinfeld, J. H., and Prather, K. A.: Flight-based chemical characterization of biomass burning aerosols within two prescribed burn smoke plumes, Atmos. Chem. Phys., 11, 12549–2565, https://https://doi.org/10.5194/acp-11-12549-2011, 2011.

Rubasinghege, G., Lentz, R. W., Scherer, M. M., and Grassian, V. H.: Simulated atmospheric processing of iron oxyhydroxide minerals at low pH: roles of particle size and acid anion in iron dissolution, P. Natl. Acad. Sci. USA, 107, 6628–6633, https://doi.org/10.1073/pnas.0910809107, 2010.

Schneider, J., Mertes, S., van Pinxteren, D., Herrmann, H., and Borrmann, S.: Uptake of nitric acid, ammonia, and organics in orographic clouds: mass spectrometric analyses of droplet residual and interstitial aerosol particles, Atmos. Chem. Phys., 17, 1571–1593, https://doi.org/10.5194/acp-17-1571-2017, 2017.

Sedwick, P. N., Sholkovitz, E. R., and Church, T. M.: Impact of anthropogenic combustion emissions on the fractional solubility of aerosol iron: Evidence from the Sargasso Sea, Geochem. Geophy. Geosy., 8, Q10Q06, https://doi.org/10.1029/2007GC001586, 2007.

See, S. W., Wang, Y. H., and Balasubramanian, R.: Contrasting reactive oxygen species and transition metal concentrations in combustion aerosols, Environ. Res., 103, 317–324, https://doi.org/10.1016/j.envres.2006.08.012, 2007.

Sellegri, K., Laj, P., Marinoni, A., Dupuy, R., Legrand, M., and Preunkert, S.: Contribution of gaseous and particulate species to droplet solute composition at the Puy de Dôme, France, Atmos. Chem. Phys., 3, 1509–1522, https://doi.org/10.5194/acp-3-1509-2003, 2003.

Shi, Z., Krom, M. D., Bonneville, S., Baker, A. R., Jickells, T. D., and Benning, L. G.: Formation of iron nanoparticles and increase in iron reactivity in mineral dust during simulated cloud processing, Environ. Sci. Technol., 43, 6592–6596, https://doi.org/10.1021/es901294g, 2009.

Shingler, T., Dey, S., Sorooshian, A., Brechtel, F. J., Wang, Z., Metcalf, A., Coggon, M., Mülmenstädt, J., Russell, L. M., Jonsson, H. H., and Seinfeld, J. H.: Characterisation and airborne deployment of a new counterflow virtual impactor inlet, Atmos. Meas. Tech., 5, 1259–1269, https://doi.org/10.5194/amt-5-1259-2012, 2012.

Song, X. H., Hopke, P. K., Fergenson, D. P., and Prather, K. A.: Classification of single particles analyzed by ATOFMS using an artificial neural network, ART-2A, Anal. Chem., 71, 860–865, https://doi.org/10.1021/ac9809682, 1999.

Sorooshian, A., Varutbangkul, V., Brechtel, F. J., Ervens, B., Feingold, G., Bahreini, R., Murphy, S. M., Holloway, J. S., Atlas, E. L., Buzorius, G., Jonsson, H., Flagan, R. C., and Seinfeld, J. H.: Oxalic acid in clear and cloudy atmospheres: analysis of data from international consortium for atmospheric research on transport and transformation 2004, J. Geophys. Res.-Atmos., 111, D23S45, https://doi.org/10.1029/2005JD006880, 2006.

Sorooshian, A., Ng, N. L., Chan, A. W. H., Feingold, G., Flagan, R. C., and Seinfeld, J. H.: Particulate organic acids and overall water-soluble aerosol composition measurements from the 2006 Gulf of Mexico Atmospheric Composition and Climate Study (GoMACCS), J. Geophys. Res.-Atmos., 112, D13201, https://doi.org/10.1029/2007JD008537, 2007.

Sullivan, R. and Prather, K.: Investigations of the diurnal cycle and mixing state of oxalic acid in individual particles in Asian aerosol outflow, Environ. Sci. Technol., 41, 8062–8069, https://doi.org/10.1021/es071134g, 2007.

Sullivan, R., Guazzotti, S., Sodeman, D., and Prather, K.: Direct observations of the atmospheric processing of Asian mineral dust, Atmos. Chem. Phys., 7, 1213–1236, https://doi.org/10.5194/acp-7-1213-2007, 2007a.

Sullivan, R. C., Guazzotti, S. A., Sodeman, D. A., Tang, Y., Carmichael, G. R., and Prather, K. A.: Mineral dust is a sink for chlorine in the marine boundary layer, Atmos. Environ., 41, 7166–7179, https://doi.org/10.1016/j.atmosenv.2007.05.047, 2007b.

Tsai, I. C., Chen, J. P., Lin, P. Y., and Wang, W. C.: Sulfur cycle and sulfate radiative forcing simulated from a coupled global climate-chemistry model, Atmos. Chem. Phys., 10, 3693–3709, https://doi.org/10.5194/acp-10-3693-2010, 2010.

Twohy, C. H. and Anderson, J. R.: Droplet nuclei in non-precipitating clouds: composition and size matter, Environ. Res. Lett., 3, 045002, https://doi.org/10.1088/1748-9326/3/4/045002, 2008.

Wu, D., Deng, X. J., Ye, Y. X., and Mao, W.: The study of fog-water chemical composition in Dayaoshan of Nanling Mountain (in Chinese), Acta Meteorol. Sin., 62, 476–485, 2004.

Yang, F., Chen, H., Wang, X., Yang, X., Du, J., and Chen, J.: Single particle mass spectrometry of oxalic acid in ambient aerosols in Shanghai: Mixing state and formation mechanism, Atmos. Environ., 43, 3876–3882, https://doi.org/10.1016/j.atmosenv.2009.05.002, 2009.

Zhang, G., Bi, X., Lou, S., Li, L., Wang, H., Wang, X., Zhou, Z., Sheng, G., Fu, J., and Chen, C.: Source and mixing state of iron-containing particles in Shanghai by individual particle analysis, Chemosphere, 95, 9–16, https://doi.org/10.1016/j.chemosphere.2013.04.046, 2014.

Zhang, G., Lin, Q., Peng, L., Bi, X., Chen, D., Li, M., Li, L., Brechtel, F.J., Chen, J., Yan, W., Wang, X., Peng, P., Sheng, G., and Zhou, Z.: The single-particle mixing state and cloud scavenging of black carbon: a case study at a high-altitude mountain site in southern China, Atmos. Chem. Phys., 17, 14975–14985, https://doi.org/10.5194/acp-17-14975-2017, 2017a.

Zhang, G., Lin, Q., Peng, L., Yang, Y., Fu, Y., Bi, X., Li, M., Chen, D., Chen, J., Cai, Z., Wang, X., Peng, P., Sheng, G., and Zhou, Z.: Insight into the in-cloud formation of oxalate based on in situ measurement by single particle mass spectrometry, Atmos, Chem. Phys., 17, 13891–13901, https://doi.org/10.5194/acp-17-13891-2017, 2017b.

Zhang, X. Y., Gong, S. L., Arimoto, R., Shen, Z. X., Mei, F. M., Wang, D., and Cheng, Y.: Characterization and temporal variation of Asian dust aerosol from a site in the northern Chinese deserts, J. Atmos. Chem., 44, 241–257, https://doi.org/10.1023/A:1022900220357, 2003.